

**Jean-Baptiste Chossat**

École de Technologie Supérieure,  
Montréal, QC H3C 1K3, Canada  
e-mail: jean-baptiste.chossat.1@ens.etsmtl.ca

**Hee-Sup Shin**

Department of Mechanical Engineering,  
Carnegie Mellon University,  
Pittsburgh, PA 15213  
e-mail: heesups@andrew.cmu.edu

**Yong-Lae Park**

Robotics Institute,  
School of Computer Science,  
Carnegie Mellon University,  
Pittsburgh, PA 15213  
e-mail: ylpark@cs.cmu.edu

**Vincent Duchaine**

École de Technologie Supérieure,  
Montréal, QC H3C 1K3, Canada  
e-mail: vincent.duchaine@etsmtl.ca

# Soft Tactile Skin Using an Embedded Ionic Liquid and Tomographic Imaging

*Whole-body-contact sensing will be crucial in the quest to make robots capable of safe interaction with humans. This paper describes a novel design and a fabrication method of artificial tactile sensing skin for robots. The manufacturing method described in this paper allows easy filling of a complex microchannel network with a liquid conductor (e.g., room temperature ionic liquid (RTIL)). The proposed sensing skin can detect the magnitude and location of surface contacts using electrical impedance tomography (EIT), an imaging technique mostly used in the medical field and examined recently in conjunction with sensors based on a piezoresistive polymer sheet for robotic applications. Unlike piezoresistive polymers, our IL-filled artificial skin changes its impedance in a more predictable manner, since the measured value is determined by a simple function of the microchannel geometry only, rather than complex physical phenomena. As a proof of concept, we demonstrate that our EIT artificial skin can detect surface contacts and graphically show their magnitudes and locations. [DOI: 10.1115/1.4029474]*

## 1 Introduction

Physical and control performance of a robot in unstructured human environments are significantly dependent on its sensing capability. As discussed by Siciliano and Khatib, whole-body-touch-sensing [1] in robots, which is still an unsolved problem, will be one of the key factors that will not only ensure human safety but also improve human-robot interactions in the future. Although the study of human tactile function has led to better understanding of the essential sensory characteristics of ideal artificial skin [2], no existing approach can match the human tactile apparatus in terms of sensitivity, multimodality, and robustness all at the same time.

One of the first attempts to produce artificial sensing skin for robotic applications was introduced by Lumelsky et al. [3,4] Their modular skin device used multiple infrared sensors to detect proximity and contact of an object. Other researchers have proposed exploiting the change in capacitance between two soft planes [5,6] or the variation in the resistance of a piezoresistive material [7–9] as means of localizing and measuring applied stresses [10]. All these approaches encounter one same challenge, complicated internal wiring to connect multiple sensing elements or to create a sensor array. In order to circumvent the associated physical constraints, the use of a flexible printed circuit board (PCB) layer or flexible/stretchable wires has been proposed. However, this method also limits the robustness of the device and its mechanical properties such as flexibility and stretchability.

We propose the use of EIT combined with a conductive liquid embedded soft sensor (Fig. 1) for tactile sensing. EIT is a noninvasive medical imaging technique that reconstructs cross-sectional images of the internal structure of a human body using impedance measurements obtained from multiple electrodes placed on the skin [11]. EIT has also been employed in tactile sensors in conjunction with piezoresistive materials as a means of detecting a contact location and its corresponding pressure [12–15]. This EIT-based tactile sensing technique simplifies the previously mentioned complicated internal wiring, since deformations caused by contact pressures on a large flexible surface can be easily measured without constraining the mechanical properties of the material.

However, the image quality obtained in this method is often relatively poor compared to those of conventional array approaches [16]. The low image quality is partially due to an ill-posed problem of the image processing [17]. Some researchers have proven that the inclusion of internal electrodes could improve image quality [18]. However, another factor is the nature of current flow in the piezoresistive materials. It has been shown that current dynamics in doped silicones are complex, nonlinear, and difficult to predict accurately [8,19,20].

Recent attempts to exploit the change in electrical resistance in soft material containing liquid metal microchannels [21] have shown promise for detecting various modalities such as strain changes [22,23], contact pressures [22,24], shear forces [25], and curvatures [26].

Unlike conventional piezoresistive rubbers based on conductive nanoparticles and involving complex interactive phenomena, the resistance of such material is dominantly governed by the change in microchannel geometry, resulting in the response to be much more predictable. Capacitive sensing can be also combined with liquid metal microchannels. Double layered microchannels with a grid pattern surrounding air pockets embedded in a silicone layer have been used to measure normal contact forces [27]. Microcontact printing has been proposed to fabricate microcomb patterns of liquid metal microchannels for detecting strain changes. Both methods utilize capacitive changes of sensing elements [28].

Following our previous work of using a soft material containing dual-liquid microchannels for detecting large strain changes with interference-free signal conduction [29], we decided to combine the advantages of the EIT sensing method with the repeatability of the mechanical deformation of microchannels filled with a conductive liquid. We used a low conductive RTIL. RTILs are not only chemically stable compared to ionic solutions (e.g., saline solutions) that are composed of water and ions but also have lower surface tensions than liquid metals (e.g., gallium-indium alloy).

We designed a matrix-type soft sensor made of silicone elastomer with embedded microchannels filled with an RTIL. Tomographic imaging allowed the sensor to detect contact location and pressure without adding internal wiring. We believe that such sensors could be useful as skin for many robotic applications. This paper describes the novel design and manufacturing processes of the proposed sensing skin (Fig. 1). Although the algorithm used for EIT image reconstruction is still crude, we are able to obtain valid imaging and believe that this approach introduces several

Manuscript received August 29, 2014; final manuscript received December 22, 2014; published online February 27, 2015. Assoc. Editor: Aaron M. Dollar.

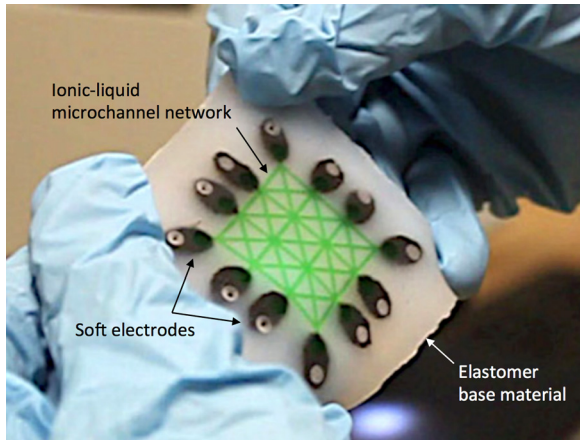


**Fig. 1 Artificial skin prototype with an embedded IL microchannel network**

advantages over previously proposed scalable tactile robotic skins.

## 2 Tomographic Imaging and IL Microchannel Embedded Silicone Sensor

Tomographic imaging is a widely used technology in medical fields, since it can provide relatively precise images of inside of a human body in a noninvasive and radiation-free way. By definition, tomographic imaging is based on the inverse reconstruction of cross-sectional images from measurements made at boundaries. Different types of measurement methods may be used depending on applications. For example, X-ray computed tomography measures X-rays going from the X-ray source to the X-ray sensors through the patient's body, while EIT measures electrical potentials of multiple measurement electrodes when an electrical current was injected through the body (see Fig. 2). The difference is that X-rays, unlike electrical currents, pass through the body in a straight line. In the case of EIT, electrical current paths are dependent on the internal conductivity of the medium and will cover the full conductive surface [12,13]. The mathematical reconstruction of EIT is thus often described as a complex and severely ill-posed problem.

The main advantage of using EIT to reconstruct the stress patterns within a piezoresistive sheet is that electrical connections only at the edges of the material are sufficient. Conductive rubber sheets generally consist of polymer matrices blended with conductive nanoparticles or microparticles. In this type of materials, electric current flows through conductive chains as a result of the quantum tunneling effect [30]. As shown in Fig. 3, unlike with bulk metal conductors, the current in a piezoresistive composite does not necessarily flow through the straight line (the shortest path) between two electrodes but rather follows the principal chains of conductive particles, which may form an arbitrary path within the rubber sheet. This means that a stress applied to a point

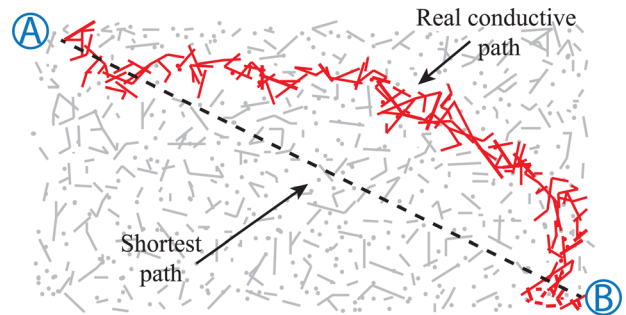


**Fig. 3 Example of a real conductive chain path that makes a longer route than a shortest path in a piezoresistive composite**

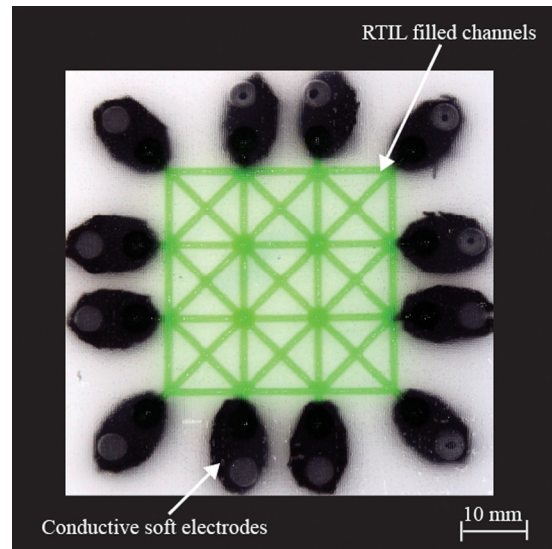


**Fig. 4 Complete skin sensor prototype. Internal lines are microchannels filled with RTIL, and black ellipses are conductive polymer patches as electrical interfaces to measurement electrodes.**

at a considerable distance from the shortest geometric path between two electrodes could change the sensor impedance more than a stress applied to a point on this line, resulting in a compromised accuracy of the contact location.

In order to solve this problem, we propose the use of a silicone sheet containing a network of microchannels filled with an IL, as shown in Fig. 4. ILs, also called molten salts, are salts in a liquid state, and unlike ionic solutions, are composed only of ions. By selecting anions and cations, it is possible to create theoretically  $10^{18}$  different ILs [31]. Some of these have melting points below room temperature, acquiring the name RTILs. This property is mainly due to the charge distribution of the ions as well as their symmetry and hydrogen bonding ability [32].

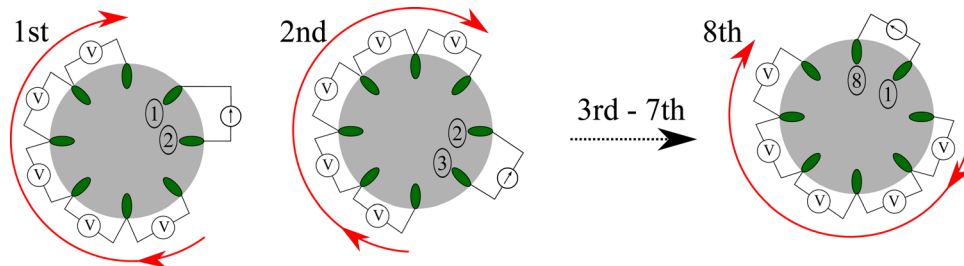


**Fig. 2 Example of a typical EIT acquisition protocol with eight electrodes. EIT requires eight consecutive current injection electrode pairs and 48 distinct voltage measurements.**

Depending on the ions used, the material properties of RTILs can be tailored with specific applications. RTILs in industry are generally considered as a “green” alternative to conventional solvents or electrolytes [32] because of their high ionic conductivity and nonvolatility [31]. These characteristics also make them suitable for use in silicone sensors [33,34].

Since silicone is gas-permeable, bubbles can form in the channels of sensors containing ionic solutions as changes in temperature increase then decrease the hydrosolubility of atmospheric gases. Water itself forms vapor as temperature increases. Avoiding the presence of water altogether is preferable. Since no general theoretical model is available to predict the properties of RTILs, most literatures rely on experimental measurements. The RTIL (1-ethyl-3-methylimidazolium ethyl sulfate (EMISE), Sigma-Aldrich/BASF,  $\geq 95\%$  purity) used in our sensor prototype has a melting point of  $-30^\circ\text{C}$  [35]. Previous research has reported that this RTIL has negligible vapor pressure and is chemically stable with contacts with both air and water [36].

It is well known that the conductivity of a channel filled with conductive liquids is a function of only the length between the two electrodes and the area of the channel cross section. Another advantage of using RTIL as a conductive medium into a resistive-based artificial skin is that its sensitivity will remain stable over time [31]. While the overall resistivity of a piezoresistive rubber is known to increase greatly with the aging of the silicone matrix [37], the resistivity of an RTIL is not affected by time [31].

Finally, ILs are also preferred to liquid metals (e.g., eutectic gallium–indium (eGaIn),  $\rho = 29.4 \times 10^{-4} \Omega \cdot \text{m}$  [38]) due to their higher resistivity ( $\rho = 2.5 \Omega \cdot \text{m}$ ), thus maximizing the variation in absolute resistance and minimizing the impact of random variations at the interface between solid and liquid.

### 3 Design and Fabrication

**3.1 Sensor Base Layer and Soft Electrodes.** Our sensor was made of an extremely soft platinum-cured silicone called Ecoflex (Smooth-on, shore 00-30) following the manufacturing process presented in Fig. 5. A mold was first machined from an acrylic sheet using an Epilog Helix 40-W  $\text{CO}_2$  laser cutter at 20% speed and 30% power. This mold bore features that produced channels of which the cross section was trapezoidal, measuring  $350 \mu\text{m}$  in depth,  $650 \mu\text{m}$  at the bottom, and  $1300 \mu\text{m}$  at the top. Larger channels than reported previously [29] were preferred in order to increase the channel volume fraction of the resulting sensor. The mold is shown in Fig. 6.

In order to avoid leakage of the ILs from the sensor due to movement of metal probes, we made silicone-based electrodes containing a mixture of high-aspect-ratio nickel strands (NiNs, length  $30 \mu\text{m}$ , Conductive Composites, Inc.) and nickel-coated micron-sized carbon fibers (NiCCF, length  $800 \mu\text{m}$ , Conductive Composites, Inc.). Nickel is highly conductive, affordable, slow to oxidize, and hence suitable for our application. This mixture provided very good conductivity with minimal impact on the mechanical properties of the silicone elastomer (e.g., high elongation at break, low hysteresis, and low Young’s modulus). It contained 4% NiNs and 0.09% NiCCF by volume, as reported previously [29]. The composite was blended for 3 min in a planetary mixer (Thinky ARE-310), which provided minimal strand agglomeration and breakage. The measured resistivity of these conductive interfaces was  $8 \times 10^3 \Omega \cdot \text{m}$ , far below the resistivity of the IL ( $\rho = 2.5 \Omega \cdot \text{m}$ ).

Twelve casted electrodes were placed in the mold described above and Ecoflex silicone was added, degassed, and then cured in an oven at  $65^\circ\text{C}$  for approximately 25 min. The cured layer was separated from the mold and the electrode surfaces that come into contact with the RTIL were etched at low power with the  $\text{CO}_2$  laser in order to expose the conductive fibers and thus increase greatly the conductivity. The wavelength of a  $\text{CO}_2$  laser

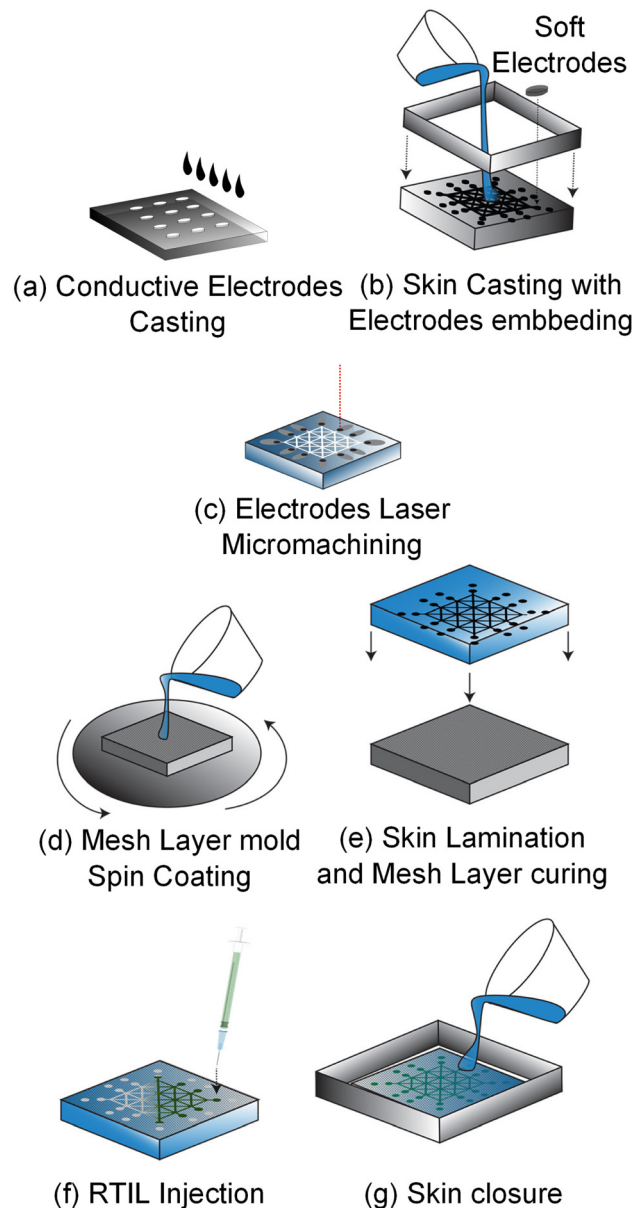


**Fig. 5 Manufacturing process. (a) Cast soft electrodes using a mixture of nickel strands and CFs with liquid silicone. (b) Pour liquid silicone to cast a base sensor layer with a microchannel pattern and embed electrodes. (c) Micromachine electrodes for increased conductivity using low-power laser. (d) Spin coat liquid silicone on a mesh layer mold. (e) Laminate the base layer on the uncured mesh layer for bonding. (f) Remove the mesh-bonded base layer from the mold and inject an RTIL. (g) Pour another silicone layer for top mesh sealing.**

( $10.6 \mu\text{m}$ ) is such that the laser is reflected by nickel and only the silicone is removed.

**3.2 Injection of RTIL Into the Sensor.** RTIL was injected into the first layer of the sensor. In previous studies, the liquid was injected into the completed assembly, using a needle to vent air from the distal end of each channel [22,29,39]. Although this technique has proven its simplicity and reliability, it allows only one-dimensional filling of a single channel in one direction and thus cannot be used for multiple interconnected channels. Indeed, in our case, it is extremely hard to completely fill the sensor array only from one injection point to one suction point, as experience shows that liquids first flow into the most friction-less path

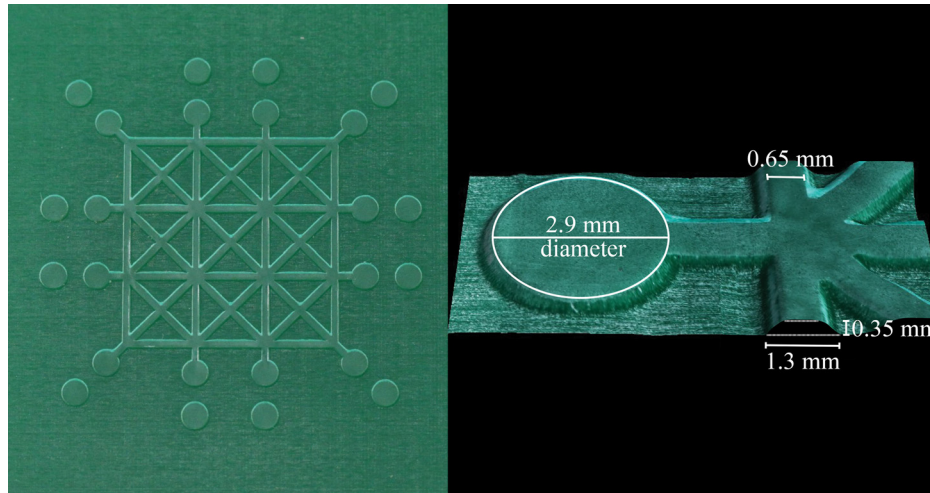


**Fig. 6** Laser cut microchannel mold (left) and its 3D microscopic view (right) of engraved details

between the two needles, resulting in empty channels in the other areas. Hence, the technique developed should allow a multidirectional filling of the channels.

Furthermore, due to the high surface tension of the liquid, combined with the hydrophobic character of silicone, filling the open channels was not possible either. Besides, the platinum-based catalyst used to cure Ecoflex is very sensitive to extraneous chemical agents, and any contact between RTIL and subsequently applied liquid silicone would inhibit curing and cause defects in the skin.

As an alternative, electrowetting [40] of the bottom surface of the channels has been investigated as a means of guiding the flow of IL into the sensor skin. However, ILs are less compliant than other liquids with electrowetting [41]. Our tests showed that the required electric field was strong enough to cause dielectric breakdown of the silicone. Freezing the liquid before curing the silicone [42] was not practical either, since the melting point of the RTIL is approximately  $-30^{\circ}\text{C}$  [35].

Our solution to the RTIL injection problem was to fabricate a silicone mesh layer that allowed air to pass through while

retaining water (like hydrophobic air filters or a Gore-Tex<sup>®</sup> material). An acrylic mold was prepared by laser micromachining using a  $\text{CO}_2$  laser engraver with minimum power to obtain a grid of cones approximately  $150\ \mu\text{m}$  in height and  $200\ \mu\text{m}$  apart, as shown in Fig. 7. A thin layer of a liquid silicone (EcoFlex 0030) was then spin-coated on the acrylic mold at 800 rpm for 30 s. Meanwhile, the first sensor layer was heated in an oven at  $65^{\circ}\text{C}$  for 10 min. The heated layer was placed on the spin-coated mold, and the assembly was placed in the oven again for curing. The skin was then carefully detached from the mold after curing maintaining the mesh layer bonded on the first sensor layer. The resulting membrane had holes approximately  $50\ \mu\text{m}$  in diameter. The skin was finally filled with RTIL using a syringe with a hypodermic needle, at room temperature, starting from one point and until all channels were filled. The needle was able to penetrate the mesh layer without damaging the net structure by taking advantage of the high stretchability of the silicone material.

When injected through a microchannel, the RTIL is constrained by the bottom and side walls. This forces the RTIL to either flow forward in the microchannel or to pass through the small holes on the top mesh layer. Although the dynamics of Newtonian liquids are usually constrained by the gravitational force, this principle does not apply any more in such small dimensions [43]. The RTIL's surface tension ( $\gamma = 48.79 \times 10^{-4}\ \text{N} \cdot \text{m}^{-1}$  [44]) therefore govern the RTIL's flow, and, with the help of the mesh layer, constrains the RTIL to flow undivided through all the networked microchannels. Indeed, the mesh layer holes are approximately 170 times smaller than the cross-sectional area of the microchannel and allow the air to vent out while being small enough to act decisively on the RTIL's surface tension.

Approximately 1 ml of RTIL was used to fill the microchannel network. We believe that this filling procedure will be useful in other fabrication and design of microfluidic sensors, especially when building complex multichannel structures.

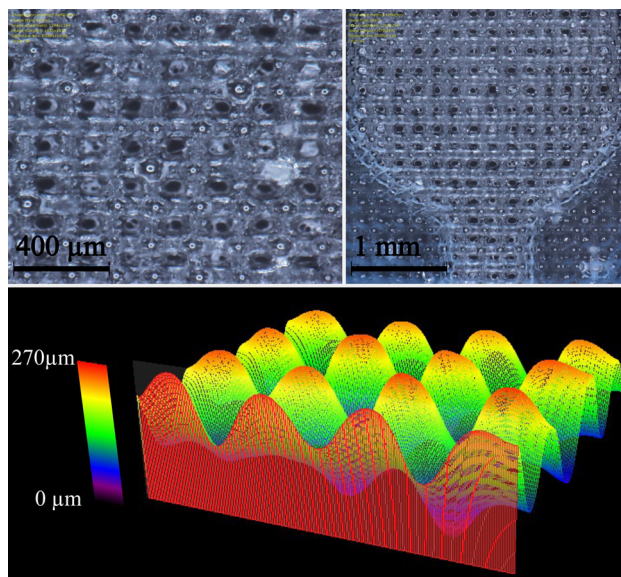


**Fig. 7** Mesh layer mold (top) and 3D image reconstitution (bottom) with an optodigital microscope (Olympus DSX-100). Color scale indicates height of structures after laser ablation.

**3.3 Sealing of the Sensor.** The netlike structure should be sealed once the sensor is filled, since wetting of the pores is possible and the RTIL could leak under external pressure. Ecoflex was mixed and degassed for 30 s and then precured for 5 min in the oven at  $65^{\circ}\text{C}$ . This increases its viscosity considerably, although it can still be poured into the enclosed space and spread carefully over the porous surface. The resulting bond was much better than what we experienced with the conventional approach of bonding two previously cured flat layer, thus insuring good robustness of the skin. This better bonding is mainly due to the geometry of the

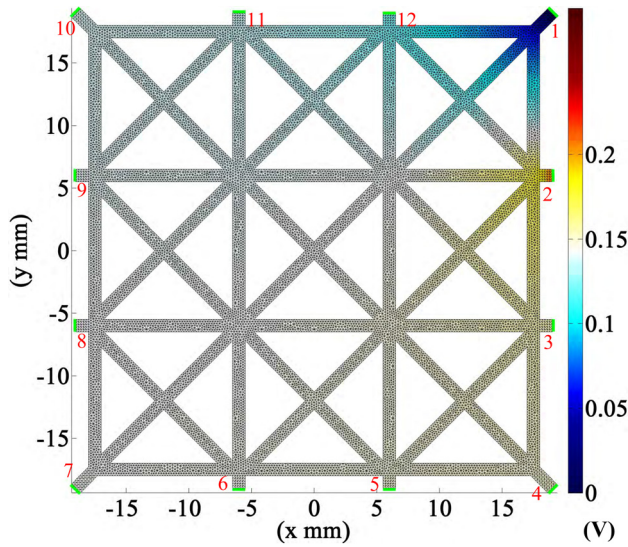


**Fig. 8 Voltage pattern from the first stimulation injecting a constant current into electrode 1 and 2. Each electrode is denoted with the green bars and is placed at the channels' extremities with its acquisition order. Right legend bar represents voltage difference in the network.**

netlike structure that increase the surface area in contact between the two layers and that also trap the uncured silicone in its pores.

Although the skin was not tested for mechanical fatigues by cyclic loading, the softness and intrinsic elasticity of Ecoflex (900% elongation at break) as well as the use of only soft or liquid components make the sensor quite robust. Moreover, unlike with the usual channel filling method, our approach did not require to create holes for liquid injection once the sensor has been sealed. Large forces (about 600 N) were applied to test our sealing methods. These caused no leakage or visible damage to the skin.

#### 4 Simulation

Before conducting experiments, we checked our EIT pressure sensing concept through simulation using an open source MATLAB toolkit (EIDORS [45]—version 3.7.1) for designing and solving an EIT model through the finite element method (FEM). A base mesh structure of the microchannel network was made in 2D using a commercial FEM software (ABAQUS/CAE 6.13-3, Dassault Systems) and exported to EIDORS.<sup>1</sup>

As illustrated in Fig. 8, EIDORS generates stimulation patterns applying a constant current to each pair of adjacent electrodes and calculates the voltage charged on each element of the mesh through a forward solver. Based on the calculated voltage, the inverse solver of EIDORS reconstructs the conductivity of the mesh and generates an image of the reconstructed conductivity [47]. The dimension of this simulation model was the same as that of the sensor prototype. The base mesh structure contains 12 electrodes (resistance: 0.2  $\Omega$ ) and a circular pressure area (diameter: 6 mm), as shown in Figs. 8 and 9, respectively.

In our simulation, the conductivity of the pressure area can be expressed as a function of the pressure derived from the following analytical model for hyperelastic pressure sensing [21]

$$\Delta R = \frac{\rho L}{wh} \left\{ \frac{1}{1 - 2(1 - \nu^2)w\chi p/Eh} - 1 \right\} \quad (1)$$

$\rho$ ,  $\nu$ , and  $E$  are the electrical resistivity of the IL, and Poisson's ratio, and elastic modulus of the silicone material, respectively.  $L$  is the length of the microchannel,  $w$  and  $h$  are the width and height

of the cross section of the microchannel, respectively. Then, based on Eq. (1), the new conductivity of the pressure area is

$$\sigma = \mu \cdot \sigma_0 \quad (2)$$

where  $\sigma_0$  is an initial conductivity and the coefficient  $\mu = 1 - 2(1 - \nu^2)w\chi p/Eh$ . Since the applied pressure has an influence on the conductivity changes of not only the pressure area but also its vicinity, in Eq. (2), the effective pressure area was calculated and used in the simulation, as illustrated in Fig. 9.

Using this conversion process, we simulated the deformation of the skin, as shown in Fig. 10. Both pressure locations and magnitudes were estimated for different pressure inputs, as shown in Fig. 10(a), using an input current of 10 mA. The following parameters were also used in the simulation:  $\sigma_0 = 0.398 \text{ S} \cdot \text{m}^{-1}$ ,  $\nu = 0.49$ , and  $E = 125 \text{ kPa}$ . 20 dB of signal-to-noise ratio was also included make a similar condition of actual sensors. The results showed the minimum conductivity at the center of the pressure and a gradual conductivity increase at the adjacent areas as the distances from the center increase reaching the initial conductivity ( $\sigma_0$ ) eventually. The conductivity reconstruction (i.e., pressure estimation) was reliable regardless of the magnitudes and the number of the pressures.

Although the current approach does not incorporate the 3D deformation of the microchannels, the simulation results demonstrated that the EIT can be easily combined with microfluidic soft sensing devices for detecting contact pressures.

#### 5 Experiments: Contact Location and Image Reconstruction

The goal of this paper is to present a novel idea of implementing EIT to touch-sensitive skin filled with an IL and to discuss the design challenges associated with this approach. The inverse EIT problem is a complex topic on which many papers have been published over the last 20 years. Future work will be oriented more toward how we can improve the touch image quality using more complex but reliable reconstruction algorithms. In the meantime, this section will present simple experiments conducted on the skin prototype in order to show that the proposed fabrication method leads to artificial skin that can effectively detect pressure contacts as well as their magnitudes.

**5.1 Sensing Mechanism of the Skin.** Given that the specific conductivity of the IL is isotropic and since the number and shape of the channels is known, the skin can be modeled as a matrix of resistors in which each channel section is a resistor and each connection between the channels is a node. The impedance of an IL is a function of the distance between electrodes, and the smallest cross-sectional area of the microchannel between the electrodes and the liquid conductivity. The pressure applied to the skin will deform the microchannel and decreases its cross-sectional area, and it consequently increases the impedance that can be measured from the electrodes located at the edge of the skin.

Since the impedance changes are due to the area changes of the cross section of the microchannel, and also the deformed silicone elastomer can easily return to its original shape when the pressure is released, the impedance changes are highly predictable and reproducible. In addition, the dynamics of ions as charge carriers are constant in a large frequency domain [33], whereas the paths of current as modified by forces applied to silicone doped with conducting nanoparticles are far more difficult to predict [8,19,20], the sensing mechanism in the our skin is more reliable than that those of EIT skin sensors that use conductive rubbers [12,13].

**5.2 EIT Image Reconstruction.** A conventional way of acquiring EIT data is measuring electrical potentials between all the electrodes except two electrodes to which an alternating

<sup>1</sup>A.vml file generated in ABAQUS was converted to a.stl file using MESHLAB [46], and then the.stl file was imported to EIDORS.

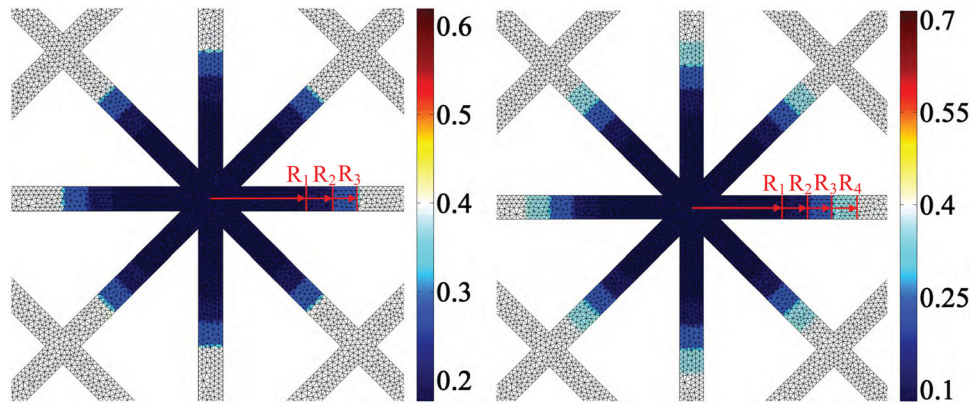


**Fig. 9** Conductivity patterns with different pressure values, 35 kPa (left) and 50 kPa (right). Legend bars represents conductivity gradient ( $S \cdot m^{-1}$ ). The coefficient  $\mu$  determines the boundary of the effective pressure area ( $R_3$  at 35 kPa and  $R_4$  at 50 kPa). At 35 kPa,  $\mu \approx 0.4433, 0.452, 0.5048,$  and  $0.7154$  for  $R_1 = 3$  mm,  $R_2 = 4$  mm, and  $R_3 = 5$  mm, respectively, and  $\mu \approx 1$  (i.e.,  $\sigma = \sigma_0$ ) for  $R_i$  ( $i \geq 4$ ); At 50 kPa,  $\mu \approx 0.2047, 0.2171, 0.2926, 0.5935,$  and  $0.8949$  for  $R_1 = 3$  mm,  $R_2 = 4$  mm,  $R_3 = 5$  mm, and  $R_4 = 6$  mm, respectively, and  $\mu \approx 1$  (i.e.,  $\sigma = \sigma_0$ ) for  $R_i$  ( $i \geq 5$ ). The coefficients are calculated based on the dimensions and material properties of the prototype.

current is injected. This process is repeated by changing the two injection electrodes until it covers all the electrodes [12,13]. Complex numerical methods may be used to reconstruct the image from the obtained data. However, in our case, we employed a

simple numerical method called *weighted filtered back projection* [48], since the purpose of our experiments was to validate the concept of using EIT on a soft skin sensor that contains a network of embedded conductive microchannels. In our method, the image

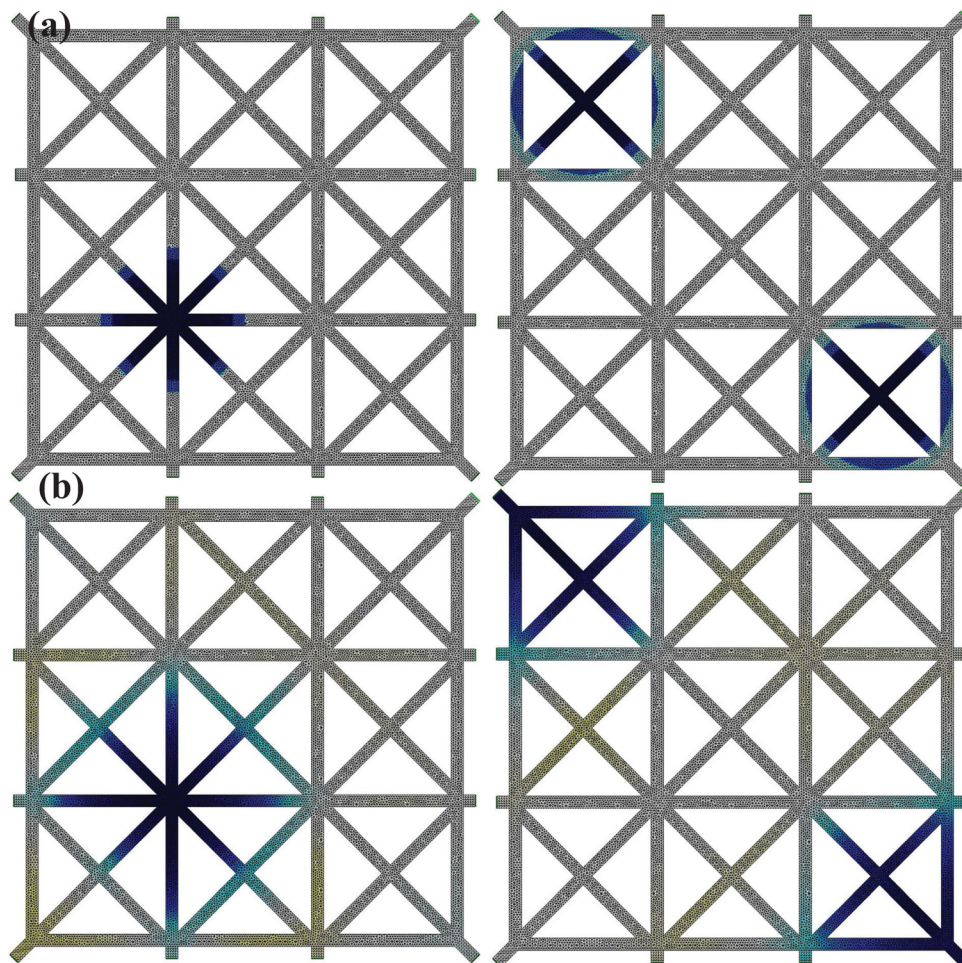


**Fig. 10** (a) Conductivity distributions with one point load ( $p = 35$  kPa) centered at ( $x = -6$  mm and  $y = -6$  mm) and two point loads ( $p = 50$  kPa) centered at ( $x = -12$  mm and  $y = 12$  mm) and ( $x = 12$  mm and  $y = -12$  mm). (b) Images of reconstructed conductivity of the loads.

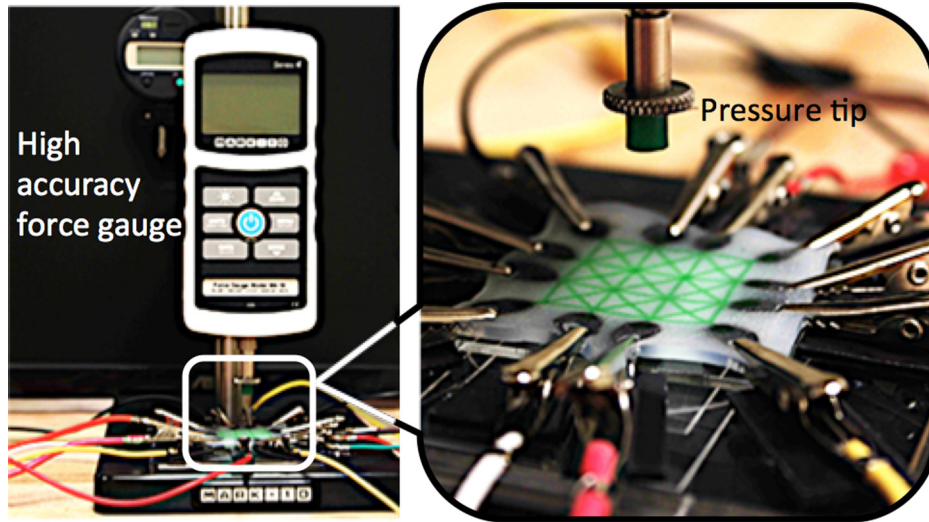


Fig. 11 Experimental setup for pressure response measurement using a high accuracy force gauge (left) and the close-up view of the sensor and the pressure tip (right)

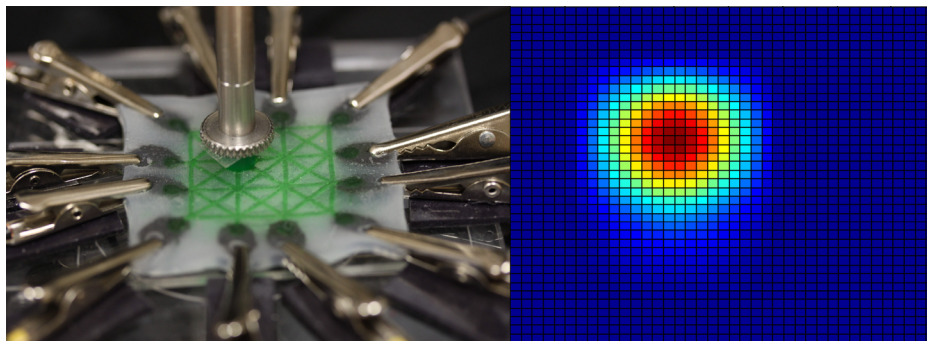


Fig. 12 Pressure application experiment (left) and its postprocessed estimated pressure image

reconstruction algorithm creates a matrix by attributing a score to each node of the skin. This score is calculated by summing the impedances of the channels crossing at this position. This simple method provides accurate results, since our skin is composed of a discrete set of channels that follow a symmetric organization as opposed to the unknown medium generally explored with EIT, thus simplifying the problem. Furthermore, the conductivity of EMISE IL is isotropic, which makes the current flow inside the channels much more predictable.

Normal forces were applied to the skin using a commercial force gauge (M4-10, Mark-10) and a test stand (ES10, Mark-10), and the impedance was measured at 1 kHz at the edge electrodes of the skin. To apply a force in a repeatable manner, a rigid cylindrical end-effector (6 mm in diameter and 6.35 mm in height) was mounted on the force gauge. Since the measurements were performed manually using an external device, a simple custom data acquisition protocol was followed. Impedance was measured between one electrode and the next, in a clockwise order, without redundancy. Measurements were performed first without any load in order to populate a calibration matrix used to evaluate the impedance due to other causes than the RTIL filled channels and mitigate their impact on the sensors' accuracy. The end-effector was then brought down to the skin until the force measured by the force gauge reached target value. The experimental setup is shown in Fig. 11.

Two experiments were conducted to evaluate the skin prototype. In the first experiment, a single load with three different force levels were applied to a same location. The skin was able to

detect both the location and the magnitude of the force, as shown in Figs. 12 and 13. For the force estimation, the resistance difference between the collected data and the calibration matrix was calculated and then filtered through bicubic interpolation in

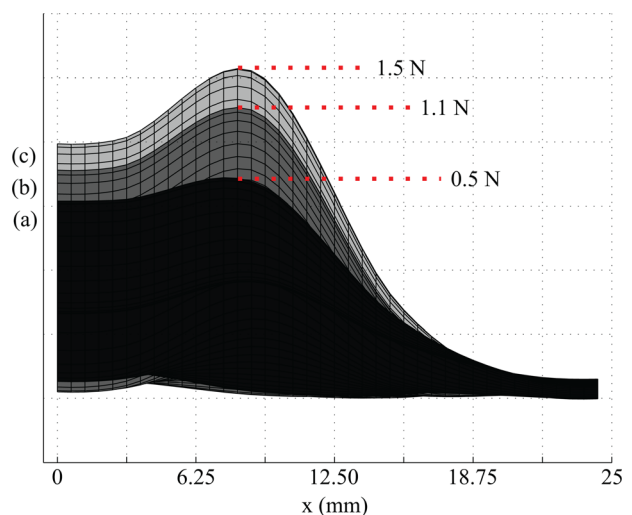
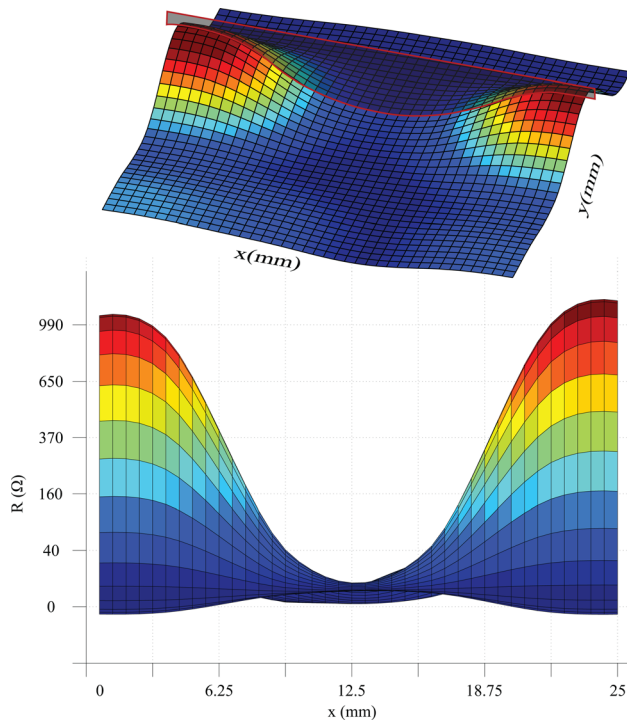


Fig. 13 MATLAB generated images of three distinct forces applied at the same skin position



**Fig. 14** MATLAB images and cross-sectional view caused by the two contact points of the force gauge end-effector with a force of 0.5 N and demonstrating skin ability to detect multiple contact location. Both images were built from the differences in resistance between the calibration matrix and the deformed skin's matrix. (The y-axis scale of both plots is not linear, since it is based on bicubic interpolation of image processing).

MATLAB. Although the experiments were simple and use only one subset of the measurements obtained, this method demonstrates the capability of extracting the location and magnitude of a contact. The contact was detected exactly at the same location of the actual load. Also, although the relationship is not exactly linear, the three different forces were estimated with the three shaded curves with peaks of different amplitudes in Fig. 13. In the second experiment, two same loads (0.5 N) were applied to the two different locations. The result, shown in Fig. 14, shows that two same resistance changes were detected at the two contact locations.

The experimental results validated that our skin prototype was able to identify the locations and magnitudes of contact forces for both single and multiple load conditions.

## 6 Conclusion

This paper describes a novel manufacturing method for a tactile skin sensor based on a noninvasive sensing approach that combines EIT with a conductive microfluidic network in a soft material.

The use microchannels filled with an IL as a contact pressure sensing element has an advantage over conductive rubber sensors since changes in resistance (or impedance) are more predictable and repeatable. Another advantage of using EIT over other common imaging techniques, such as arrayed electrodes [49], is that it provides a complete cross-sectional image. Also, the spatial resolution of the sensor depends more on the density of the conductive channels of the network rather than on the number of electrodes that typically determines the spatial resolution of conventional grid-patterned tactile sensors. The complexity and density of the network can be easily reconfigurable without changing the number of signal wires.

We described the design and a method of manufacturing for a soft tactile skin with 12 electrodes. The result demonstrated that the skin prototype could provide clear images of contact pressures

on the surface using EIT imaging. Although the current prototype is small-sized, our approach is scalable in terms of the size of the skin and its resolution within the limits of the fabrication equipment (e.g., the size of the laser cutter and the spin-coater). The manufacturing of molds and the use of fast-curing soft silicone allowed complete tailoring of various parameters such as size, shape, number of elements, and resolution of a contact area over the sensing region.

We believe that the inherent softness of silicone, the conductive properties of EMISE, and the simplicity of the manufacturing procedure enabled this conformable skin, an interesting avenue to explore for the development of highly flexible and stretchable large-area tactile sensing skin for robotic applications. Future work will be focused on the development of an analytical model of the impedance of the skin to improve the quality of the image reconstruction.

## References

- [1] Siciliano, B., and Khatib, O., 2008, *Springer Handbook of Robotics*, Springer-Verlag, Berlin, Germany.
- [2] Dargahi, J., and Najarian, S., 2004, "Human Tactile Perception as a Standard for Artificial Tactile Sensing—A Review," *Int. J. Med. Rob. Comput. Assist. Surg.*, **1**(1), pp. 23–35.
- [3] Cheung, E., and Lumelsky, V., 1989, "Development of Sensitive Skin for a 3D Robot Arm Operating in an Uncertain Environment," *IEEE International Conference on Robotics and Automation*, Scottsdale, AZ, May 14–19, pp. 1056–1061.
- [4] Lumelsky, V. J., Shur, M. S., and Wagner, S., 2001, "Sensitive Skin," *IEEE Sens. J.*, **1**(1), pp. 41–51.
- [5] Cannata, G., Maggiali, M., Metta, G., and Sandini, G., 2008, "An Embedded Artificial Skin for Humanoid Robots," *IEEE International Conference on Multi-sensor Fusion and Integration for Intelligent Systems (MFI 2008)*, Seoul, South Korea, Aug. 20–22, pp. 434–438.
- [6] Ulmen, J., and Cutkosky, M., 2010, "A Robust, Low-Cost and Low-Noise Artificial Skin for Human-Friendly Robots," *IEEE International Conference on Robotics and Automation (ICRA)*, Anchorage, AK, May 3–7, pp. 4836–4841.
- [7] Duchaine, V., Lauzier, N., Baril, M., Lacasse, M.-A., and Gosselin, C., 2009, "A Flexible Robot Skin for Safe Physical Human Robot Interaction," *IEEE International Conference on Robotics and Automation (ICRA'09)*, Kobe, Japan, May 12–17, pp. 3676–3681.
- [8] Lacasse, M.-A., Duchaine, V., and Gosselin, C., 2010, "Characterization of the Electrical Resistance of Carbon-Black-Filled Silicone: Application to a Flexible and Stretchable Robot Skin," *IEEE International Conference on Robotics and Automation (ICRA)*, Anchorage, AK, May 3–7, pp. 4842–4848.
- [9] Shimojo, M., Namiki, A., Ishikawa, M., Makino, R., and Mabuchi, K., 2004, "A Tactile Sensor Sheet Using Pressure Conductive Rubber With Electrical-Wires Stitched Method," *IEEE Sens. J.*, **4**(5), pp. 589–596.
- [10] Cutkosky, M. R., and Ulmen, J., 2014, "Dynamic Tactile Sensing," *The Human Hand as an Inspiration for Robot Hand Development*, Springer International Publishing, Cham, Switzerland, pp. 389–403.
- [11] Geselowitz, D. B., 1971, "An Application of Electrocardiographic Lead Theory to Impedance Plethysmography," *IEEE Trans. Biomed. Eng.*, **18**(1), pp. 38–41.
- [12] Nagakubo, A., Alirezai, H., and Kuniyoshi, Y., 2007, "A Deformable and Deformation Sensitive Tactile Distribution Sensor," *IEEE International Conference on Robotics and Biomimetics (ROBIO 2007)*, Sanya, China, Dec. 15–18, pp. 1301–1308.
- [13] Kato, Y., Mukai, T., Hayakawa, T., and Shibata, T., 2007, "Tactile Sensor Without Wire and Sensing Element in the Tactile Region Based on EIT Method," *Sixth IEEE Sensors Conference*, Atlanta, GA, Oct. 28–31, pp. 792–795.
- [14] Elsanadedy, A., 2012, "Application of Electrical Impedance Tomography to Robotic Tactile Sensing," Ph.D. thesis, Carleton University, Ottawa, Canada.
- [15] Tawil, D. S., Rye, D., and Velonaki, M., 2009, "Improved EIT Drive Patterns for a Robotics Sensitive Skin," *Proceeding of Australasian Conference on Robotics and Automation (ACRA)*, Sydney, Australia, Dec. 2–4.
- [16] Someya, T., Sekitani, T., Iba, S., Kato, Y., Kawaguchi, H., and Sakurai, T., 2004, "A Large-Area, Flexible Pressure Sensor Matrix With Organic Field-Effect Transistors for Artificial Skin Applications," *Proc. Natl. Acad. Sci. U.S.A.*, **101**(27), pp. 9966–9970.
- [17] Kao, T.-J., Isaacson, D., Newell, J., and Saulnier, G., 2006, "A 3D Reconstruction Algorithm for EIT Using a Handheld Probe for Breast Cancer Detection," *Physiol. Meas.*, **27**(5), p. S1.
- [18] Tawil, D. S., Rye, D., and Velonaki, M., 2011, "Improved Image Reconstruction for an EIT-Based Sensitive Skin With Multiple Internal Electrodes," *IEEE Trans. Rob.*, **27**(3), pp. 425–435.
- [19] Kost, J., Foux, A., and Narkis, M., 1994, "Quantitative Model Relating Electrical Resistance, Strain, and Time for Carbon Black Loaded Silicone Rubber," *Polym. Eng. Sci.*, **34**(21), pp. 1628–1634.
- [20] Ding, T., Wang, L., and Wang, P., 2007, "Changes in Electrical Resistance of Carbon-Black-Filled Silicone Rubber Composite During Compression," *J. Polym. Sci., B: Polym. Phys.*, **45**(19), pp. 2700–2706.
- [21] Park, Y.-L., Majidi, C., Kramer, R., Bérard, P., and Wood, R. J., 2010, "Hyperelastic Pressure Sensing With a Liquid-Embedded Elastomer," *J. Micro-mech. Microeng.*, **20**(12), p. 125029.

- [22] Park, Y.-L., Chen, B.-R., and Wood, R. J., 2012, "Design and Fabrication of Soft Artificial Skin Using Embedded Microchannels and Liquid Conductors," *IEEE Sens. J.*, **12**(8), pp. 2711–2718.
- [23] Park, Y.-L., Chen, B.-R., Pérez-Arancibia, N. O., Young, D., Stirling, L., Wood, R. J., Goldfield, E. C., and Nagpal, R., 2014, "Design and Control of a Bio-Inspired Soft Wearable Robotic Device for Ankle–Foot Rehabilitation," *Bioinspiration Biomimetics*, **9**(1), p. 016007.
- [24] Park, Y.-L., Tepayotl-Ramirez, D., Wood, R. J., and Majidi, C., 2012, "Influence of Cross-Sectional Geometry on the Sensitivity and Hysteresis of Liquid-Phase Electronic Pressure Sensors," *Appl. Phys. Lett.*, **101**(19), p. 191904.
- [25] Vogt, D. M., Park, Y.-L., and Wood, R. J., 2013, "Design and Characterization of a Soft Multi-Axis Force Sensor Using Embedded Microfluidic Channels," *IEEE Sens. J.*, **13**(10), pp. 4056–4064.
- [26] Majidi, C., Kramer, R., and Wood, R., 2011, "A Non-Differential Elastomer Curvature Sensor for Softer-Than-Skin Electronics," *Smart Mater. Struct.*, **20**(10), p. 105017.
- [27] Wong, R. D. P., Posner, J. D., and Santos, V. J., 2012, "Flexible Microfluidic Normal Force Sensor Skin for Tactile Feedback," *Sens. Actuators, A*, **179**(4), pp. 62–69.
- [28] Tabatabai, A., Fassler, A., Usiak, C., and Majidi, C., 2013, "Liquid-Phase Gallium–Indium Alloy Electronics With Microcontact Printing," *Langmuir*, **29**(20), pp. 6194–6200.
- [29] Chossat, J.-B., Park, Y.-L., Wood, R., and Duchaine, V., 2013, "A Soft Strain Sensor Based on Ionic and Metal Liquids," *IEEE Sens. J.*, **13**(9), pp. 3405–3414.
- [30] Hu, N., Karube, Y., Yan, C., Masuda, Z., and Fukunaga, H., 2008, "Tunneling Effect in a Polymer/Carbon Nanotube Nanocomposite Strain Sensor," *Acta Mater.*, **56**(13), pp. 2929–2936.
- [31] Visser, A. E., Bridges, N. J., and Rogers, R. D., 2009, *Ionic Liquids: Science and Applications*, Oxford University Press, Cambridge, UK.
- [32] Marsh, K., Boxall, J., and Lichtenthaler, R., 2004, "Room Temperature Ionic Liquids and Their Mixtures—A Review," *Fluid Phase Equilibria*, **219**(1), pp. 93–98.
- [33] Zhu, Y., Chao, C., Cheng, C.-H., and Leung, W.-F., 2009, "A Novel Ionic-Liquid Strain Sensor for Large-Strain Applications," *IEEE Electron Device Lett.*, **30**(4), pp. 337–339.
- [34] Noda, K., Iwase, E., Matsumoto, K., and Shimoyama, I., 2010, "Stretchable Liquid Tactile Sensor for Robot-Joints," IEEE International Conference on Robotics and Automation (ICRA), Anchorage, AK, May 3–7, pp. 4212–4217.
- [35] ChemSpider, 2014, "1-Ethyl-3-Methylimidazolium Ethyl Sulfate," Royal Society of Chemistry, Cambridge, UK, accessed on Nov. 17, 2014, <http://www.chemspider.com/Chemical-Structure.16144279.html?rid=a6400a19-0943-4419-a840-845b6fa29630>
- [36] Zuo, G., Zhao, Z., Yan, S., and Zhang, X., 2010, "Thermodynamic Properties of a New Working Pair: 1-Ethyl-3-Methylimidazolium Ethylsulfate and Water," *Chem. Eng. J.*, **156**(3), pp. 613–617.
- [37] Ying, H., Xiulan, F., Min, W., Panfeng, H., and Yunjian, G., 2007, "Research on Nano-SiO<sub>2</sub>/Carbon Black Composite for Flexible Tactile Sensing," IEEE International Conference on Information Acquisition, (ICIA'07), Seogwipo-si, South Korea, July 8–11, pp. 260–264.
- [38] Dickey, M. D., Chiechi, R. C., Larsen, R. J., Weiss, E. A., Weitz, D. A., and Whitesides, G. M., 2008, "Eutectic Gallium–Indium (EGaIn): A Liquid Metal Alloy for the Formation of Stable Structures in Microchannels at Room Temperature," *Adv. Funct. Mater.*, **18**(7), pp. 1097–1104.
- [39] Kramer, R. K., Majidi, C., and Wood, R. J., 2011, "Wearable Tactile Keypad With Stretchable Artificial Skin," IEEE International Conference on Robotics and Automation (ICRA), Shanghai, China, May 9–13, pp. 1103–1107.
- [40] Lee, J., Moon, H., Fowler, J., Schoellhammer, T., and Kim, C.-J., 2002, "Electrowetting and Electrowetting-on-Dielectric for Microscale Liquid Handling," *Sens. Actuators, A*, **95**(2), pp. 259–268.
- [41] Dubois, P., Marchand, G., Fouillet, Y., Berthier, J., Douki, T., Hassine, F., Gmouh, S., and Vaultier, M., 2006, "Ionic Liquid Droplet as e-Microreactor," *Anal. Chem.*, **78**(14), pp. 4909–4917.
- [42] Fassler, A., and Majidi, C., 2013, "3D Structures of Liquid-Phase Gallium Alloy Embedded in PDMS With Freeze Casting," *Lab Chip*, **13**, pp. 4442–4450.
- [43] Lambert, P., 2013, *Surface Tension in Microsystems—Engineering Below the Capillary Length*, Springer, Dordrecht, The Netherlands.
- [44] Yang, J.-Z., Lu, X.-M., Gui, J.-S., and Xu, W.-G., 2004, "A New Theory for Ionic Liquids—The Interstice Model Part I. The Density and Surface Tension of Ionic Liquid EMISE," *Green Chem.*, **6**(11), pp. 541–543.
- [45] Alder, A., and Lionheart, W. R. B., 2006, "Uses and Abuses of EIDORS: An Extensible Software Base for EIT," *Physiol. Meas.*, **27**(5), pp. S25–S42.
- [46] "MeshLab," <http://meshlab.sourceforge.net>
- [47] Vauhkonen, M., Lionheart, W. R., Heikkinen, L. M., Vauhkonen, P. J., and Kaipio, J. P., 2001, "A MATLAB Package for the EIDORS Project to Reconstruct Two-Dimensional EIT Images," *Physiol. Meas.*, **22**(1), pp. 107–112.
- [48] Kotre, C., 1994, "EIT Image Reconstruction Using Sensitivity Weighted Filtered Backprojection," *Physiol. Meas.*, **15**(2A), pp. A125–A136.
- [49] Lipomi, D. J., Vosgueritchian, M., Tee, B. C., Hellstrom, S. L., Lee, J. A., Fox, C. H., and Bao, Z., 2011, "Skin-Like Pressure and Strain Sensors Based on Transparent Elastic Films of Carbon Nanotubes," *Nat. Nanotechnol.* **6**(12), pp. 788–792.